

EFFECTS OF THE CORE-COLLAPSE SUPERNOVA EJECTA IMPACT ON A RAPIDLY ROTATING MASSIVE COMPANION STAR

CHUNHUA ZHU¹, GUOLIANG LÜ¹, ZHAOJUN WANG¹

¹School of Physical Science and Technology, Xinjiang University, Urumqi, 830046, China.

ABSTRACT

We investigate the effects of the core-collapse supernova ejecta on a rapidly rotating and massive companion star. We show that the stripped mass raises by twice when compare with a massive but non-rotating companion star. In close binaries with orbital periods of about 1 day, the stripped masses reach up to $\sim 1M_{\odot}$. By simulating the evolutions of the rotational velocities of the massive companion stars based on different stripped masses, we find that the rotational velocity decreases greatly for stripped mass that is higher than about $1M_{\odot}$. Of all the known high mass X-ray binaries (HMXBs), Cygnus X-3 and 1WGA J0648.024418 have the shortest orbital periods of 0.2 and 1.55 days, respectively. The optical counterpart of the former is a Wolf-Rayet star, whereas it is a hot subdwarf for the latter. Applying our model to the two HMXBs, we suggest that the hydrogen-rich envelopes of their optical counterparts may have been stripped by CCSN ejecta.

Keywords: binaries: close — X-rays: binaries — star: evolution

1. INTRODUCTION

High mass X-ray binaries (HMXBs) are composed of a compact object (CO) and a massive companion star of OB spectral type whose matter is accreted onto the CO. The CO is usually a neutron star (NS) or a black hole (BH). HMXBs are divided into BeHMXBs and sgHMXBs. In the former, the companions of accreting COs are Be stars, whereas they are supergiants in the latter. Of the 114 HMXBs known in the Galaxy (Liu et al. 2006), about 32% are sgHMXBs and more than 60% are BeHMXBs. Supergiant fast X-ray transients (SFXTs) are a subclass of sgHMXBs. They are characterized by sporadic, short and intense X-ray fares. There are about 10 SFXTs known in the Galaxy (e. g., Romano et al. 2014). In the Small Magellanic Cloud, 148 are confirmed candidates of HMXBs (Haberl & Sturm 2016), in which only SMC X-1 belongs to sgHMXBs while others are BeHMXBs. Antoniou & Zezas (2016) classified 40 HMXBs in the Large Magellanic Cloud and found 33 BeHMXBs and 4 sgHMXBs, including two systems in which the COs may be BHs. Usually, the progenitors of HMXBs undergo core-collapse supernovae (CCSNe). When COs form, CCSN ejecta collides with their companion stars. It was shown by many literatures that the interaction of CCSN ejecta with the companion star may affect the evolution of the latter if the orbital periods are short enough

(e. g., Wheeler et al. 1975; Hirai et al. 2014; Liu et al. 2015). Using two-dimensional (2D) hydrodynamical simulations, Hirai et al. (2014) found that up to 25% of the companions mass can be stripped for the shortest binary separations, whereas Liu et al. (2015) suggested that at most 10% of the companions mass is removed based on 3D hydrodynamical simulations. The stripped mass depends greatly on binary separations.

Figure 1 shows the distribution of the Galactic HMXBs orbital periods. Obviously, there are 17 HMXBs with orbital period shorter than 10 days. In particular, the orbital period of Cygnus X-3 is only 0.2 days (Parsignault et al. 1972), and its optical counterpart, V1521 Cyg, is a Wolf-Rayet star (van Kerkwijk et al. 1992). Similarly, 1WGA J0648.024418 has an orbital period of 1.55 days (Thackeray 1970) with an optical counterpart of a hydrogen-depleted subdwarf O6 (HD 49798). In the remaining 15 HMXBs, their optical counterparts are supergiants, that is, they are sgHMXBs (Liu et al. 2006; Romano et al. 2014). Based on Wheeler et al. (1975), Hirai et al. (2014) and Liu et al. (2015), these optical counterparts should be greatly affected by the ejecta of supernovae. However, to our knowledge, the effects of CCSN ejecta on the companion star are seldom considered in previous literatures on HMXBs. As Shao & Li (2014) showed, the companion stars may have been spun up and become Be stars before COs were formed in HMXBs with short orbital periods. When CCSNe occur, a certain amount of mass should be

†zhuchunhua@xju.edu.cn, guolianglv@xao.ac.cn

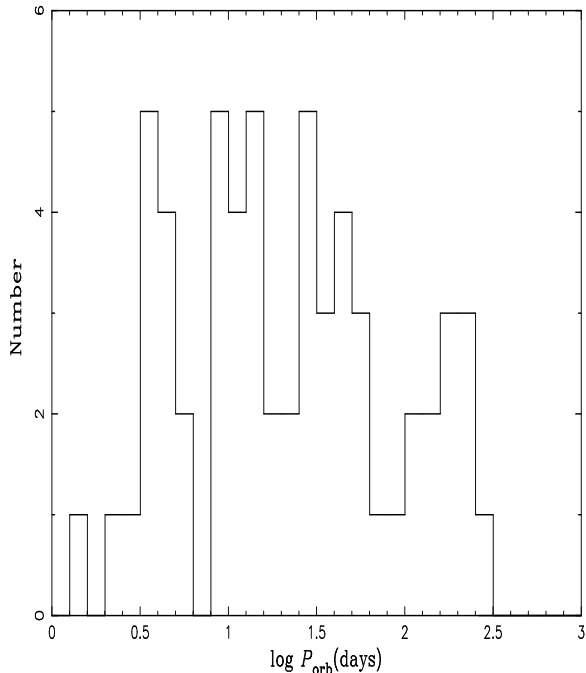


Figure 1. Orbit periods of HMXBs in the Milky Way based on the observational data from Liu et al. (2006) and Romano et al. (2014).

removed from these Be stars. We ask the questions: How does the surface velocity of these Be stars evolve? Are these Be stars remain Be stars after the redistributions of angular momentum?

In this paper, we investigate the impact of CCSN ejecta on their rotating massive companion stars, and try to understand the optical counterparts of HMXBs. §2 describes the stellar model we use for simulating the evolution of rotating stars. The stripped masses from rotating massive stars during CCSN are estimated in §3, and the evolutions of rotating massive stars after stripped masses are shown in §4. We present the main conclusions in §5.

2. BE STARS AND THE EVOLUTION OF ROTATING STARS

Be stars are B type stars with very high rotational velocity, close to the critical velocity (V_{crit}) where gravity is balanced by the centrifugal force. A review of Be stars can be seen in Porter & Rivinius (2003). In HMXBs, Be stars, which originate from main sequence (MS) stars, accrete matter from their companion stars. A detailed investigations and their properties of Be stars can be found in the works by de Mink et al. (2013), Shao & Li (2014) and Reig (2011). The range of mass distribution for Be stars in HMXBs is between 8 and 22 M_{\odot} (Chaty 2013). For simplicity, in this work, we define phenomenologically a MS star as Be star if its mass is between 8 and 22 M_{\odot} and its rotational velocity is higher than 80% of V_{crit} (Porter & Rivinius 2003).

Rotation has significant effects on the massive stars (Maeder & Meynet 2000). Here, we use MESA (version 8118, Paxton et al. 2011, 2013, 2015) to compute the structures and evolutions of rotating massive stars. By considering the physics of rotation, mass loss and magnetic fields, Brott et al. (2011) gave the grids of evolutionary models for rotating massive stars. In order to compare with their results, we use similar input parameters and criteria in MESA: The Ledoux criterion is used for convection, mixing-length parameter (α_{LMT}) is taken as 1.5, an efficiency parameter (α_{SEM}) of unity is assumed for semi-convection. The metallicity (Z) of the Milky Way is taken as 0.0088 in Brott et al. (2011), which is lower than that of the Sun ($Z_{\odot} = 0.012$) found by Asplund et al. (2005).

The mass-loss rate is calculated via the model given by Vink et al. (2001). Due to rotation, the mass-loss rate is enhanced and given by (Langer 1998)

$$\dot{M} = \left(\frac{1}{1 - \Omega/\Omega_{\text{crit}}} \right)^{\beta} \dot{M}^0, \quad (1)$$

where Ω and Ω_{crit} are the angular velocity and the critical angular velocity, respectively, and $\beta = 0.43$ (Langer 1998).

Rotation induces instability of various kinds, such as dynamical shear instability, Solberg-Hilòland instability, secular shear instability, Eddington-Sweet circulation, and the Goldreich-Schubert-Fricke instability (e.g., Heger et al. 2000), which results in the transport of angular momentum (e.g., Endal & Sofia 1978; Pinsonneault et al. 1989; Heger et al. 2000). Following Brott et al. (2011), the ratio of the turbulent viscosity to the diffusion coefficient (f_c) is taken as 0.0228 (Heger et al. 2000), and the ratio of sensitivity to chemical gradients (f_{μ}) as 0.1 (Yoon et al. 2006).

Figure 2 shows the evolution of a star with initial mass of 15 M_{\odot} on the MS phase. It is obvious that, for the models with low initial rotational velocity ($V_i = 223$ km s^{-1}), the results calculated by MESA and Brott et al. (2011) are in excellent agreement although there are small differences in luminosity and radius. However, this is not the case in models for high V_i of 595 km s^{-1} , where the results of MESA are quite different from those in Brott et al. (2011). Especially, when V_i increases from 223 to 595 km s^{-1} , Brott et al. (2011) predicted a prolong in the lifetime of MS by about 30% whereas a prolong of only about 10% is predicted in MESA. Furthermore, the rotational velocity (V_s) calculated by MESA decreases more rapidly than that using the model of Brott et al. (2011). In this work, we do not discuss the details that result in these differences, but one should note that they may lead to some large uncertainties in simulating rapidly rotating massive stars.

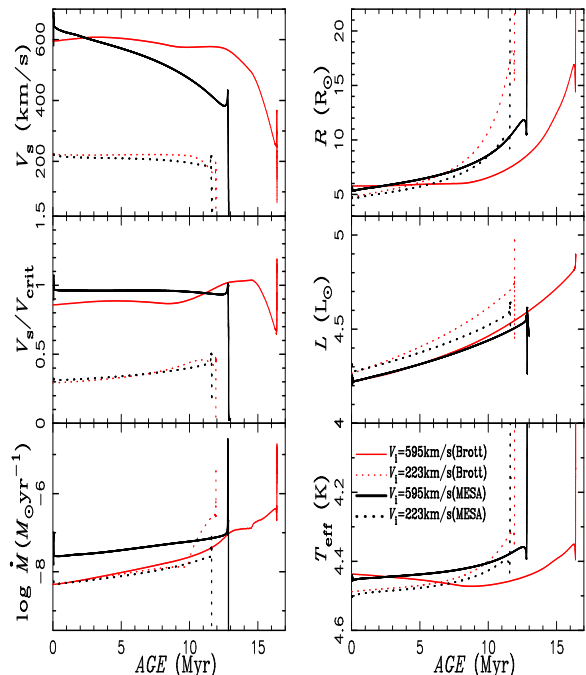


Figure 2. The evolutions of physical parameters for a star with initial mass of $15 M_{\odot}$ on the MS phase. V_s and V_{crit} are the rotational velocity on the stellar surface and the critical rotational velocity, respectively. V_i represents the initial value of V_s . Different V_i is represented by different linetypes which are shown in the legend in the bottom right plot. The brackets indicate that the data are either taken from the grids of Brott et al. (2011) or calculated by MESA.

3. CORE-COLLAPSE SUPERNOVAE

3.1. Effects of Core-Collapse Supernovae on Orbital Periods

Due to an asymmetry during CCSN, a new-born NS receives a kick velocity (v_k) which may disrupt the binary system. Brandt & Podsiadlowski (1995) systematically studied the effects of the kick velocity on the orbital periods. They found that post-CCSN distributions for binary parameters, such as orbital period, eccentricity, are determined by numerous factors including pre-CCSN orbital period, eccentricity and stellar masses, post-CCSN stellar masses, the magnitude and direction of the kick velocity. As shown in Figure 1 in Belczynski et al. (2008), the pre-CCSN masses of NS progenitors are between about 6 and $10 M_{\odot}$ using the mass-loss rates in Nieuwenhuijzen & de Jager (1990), Kudritzki & Reimers (1978) and Vassiliadis & Wood (1993) for H-rich stars on MS, red giant and asymptotic giant branches, respectively. For simplicity, we assume the pre-CCSN masses to be $8 M_{\odot}$ for all NS progenitors, and $1.4 M_{\odot}$ as the mass for all new-born NSs (Belczynski et al. 2008; Lattimer & Prakash 2007). As binary systems usually have undergone binary interaction, such as mass transfer or tidal interaction, the pre-CCSN eccentricity before CCSNe occur is taken

as 0. Of course, a new-born BH also obtains a kick velocity. However, there is no observational evidence for it. Therefore, we assume that the kick velocities for BHs are similar to those of NSs. Based on Figure 1 in Belczynski et al. (2008), we take $10 M_{\odot}$ as the pre-CCSN masses for all BH progenitors, and the masses for all new-born BHs as $8 M_{\odot}$. Hence, in this paper, the binary parameters for post-CCSN systems are assumed dependent on the magnitude and direction of the kick velocity.

Based on the measured proper motions for 233 pulsars, Hobbs et al. (2005) found that the distribution of kick velocities can be perfectly described by a Maxwellian distribution

$$P(v_k) = \sqrt{\frac{2}{\pi}} \frac{v_k^2}{\sigma_k^3} e^{-v_k^2/2\sigma_k^2}. \quad (2)$$

with a dispersion of $\sigma_k = 265 \text{ km s}^{-1}$. This implies that the direction of kick velocity is uniform over all solid angles.

For a given pre-CCSN binary, we can determine the distribution for values and directions of kick velocities using Monte Carlo method, and calculate the probability of survival for a system after CCSN, and its binary parameters. A detailed description and the codes for the above calculations can be found in Hurley et al. (2002).

In this work, we use the codes provided by Hurley et al. (2002) to calculate the binary parameters of post-CCSN systems. Considering that the orbital periods of HMXBs are between 0.2 and 300 day (See Figure 1), we take a similar range for the orbital periods (P_i) of pre-CCSN systems. Figure 3 shows the percentage of bound remaining in binaries after CCSNe. Here, $\Delta \log P_i = 0.1$ day, and 10000 binary systems are calculated for every orbital period. The results show that the larger the orbital period for a pre-CCSN binary is, the more easily the binary is disrupted. The smaller the masses for the companions of CO' progenitors in pre-CCSN binaries are, the more difficult for the binaries to survive. Since the masses of new-born BHs ($\sim 8 M_{\odot}$) are larger than those of new-born NSs ($\sim 1.4 M_{\odot}$), hence, for the same orbital periods, the binaries that produce BHs will remain bounded more readily than those that produce NSs.

Figure 4 gives the distribution of pre- and post-CCSN orbital periods. It is clear that the range of orbital period in a post-CCSN binary is wider. The post-CCSN binaries with orbital periods shorter than 10 days may originate from pre-CCSN binaries with orbital periods shorter than about 30 days. By comparing the left panel to the right panel in Figure 4, the changes in orbital periods from pre- to post-CCSN are similar regardless of whether CCSN produces BHs or NSs.

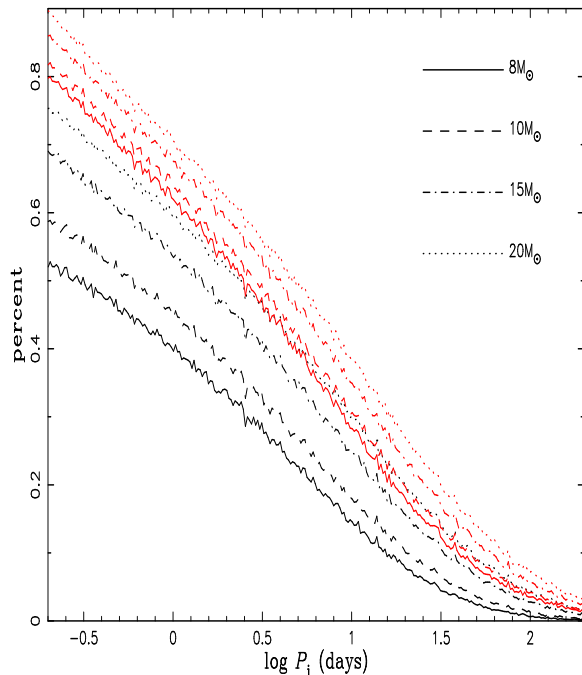


Figure 3. The percentage of bound remaining binaries after CCSNe. P_i is the pre-CCSN orbital period. The black and red lines represent that COs are the NSs and BHs, respectively.

3.2. Impact of Core-collapse Supernovae on Rotating Massive Stars

CCSNe do not only affect the orbital periods of binaries, but also have impact on the companion stars of new-born CO progenitors (e.g., Wheeler et al. 1975; Marietta et al. 2000; Pan et al. 2012; Shappee et al. 2013; Liu et al. 2015). At the beginning of CCSN ejecta colliding with the companion stars, a shock is sent into the stellar envelope of the latter, and, simultaneously, a reverse shock is sent back into the former. The shock propagates throughout the companion star, while the reverse shock turns into a bow shock around the companion star. The results of the impact of the CCSN ejecta on the companion star is that much of the shock energy is deposited in the companion’s envelope which turns into internal energy causing the companion star to heat up. If the internal energy of the material in the companion’s envelope is high enough, it is stripped away from the companion star.

The stripped mass is determined by local total energy given by Marietta et al. (2000),

$$E_{\text{tot}} = E_{\text{kin}} + E_{\text{in}} + E_{\text{gr}}, \quad (3)$$

where E_{kin} , E_{in} and E_{gr} are the specific kinetic energy, the specific internal energy, and the specific potential energy, respectively. The first and second are positive, while the third is negative. Matter is stripped if $E_{\text{tot}} > 0$.

Pan et al. (2012) found that the final stripped mass

can be estimated using the power law given by

$$M_{\text{st}} = A \left(\frac{a}{R_2} \right)^\eta M_2, \quad (4)$$

where R_2 and M_2 are radius and mass of the companion star, respectively, and a is the binary separation. Here, A and η are fitting parameters whose values are dependent on the properties of CCSNe (including energy, mass and velocity of ejecta), the structure of companion stars (including radius, density profile) and binary separations (e.g., Pan et al. 2012). Both Hirai et al. (2014) and Liu et al. (2015) estimated the stripped masses from the companion stars during CCSNe. The former focused on the red-giant companion stars, while the latter investigated the MS companion stars. The detailed structures of a red-giant companion star are very different from stars in the MS phase. Therefore, $A = 0.26$ and $\eta = -4.3$ are taken in Hirai et al. (2014), while they are 0.143 and -2.65 , respectively, in Liu et al. (2015). Although we focus on MS stars, we take the value for fitting parameters (A and η) from both in Hirai et al. (2014) and Liu et al. (2015) to estimate the stripped masses in order to discuss the effects of M_{st} on rotating massive stars.

Simultaneously, the shock heating can change the internal structures of the companion stars. However, it is beyond the scope of this work to calculate M_{st} by 2D or 3D hydrodynamical simulations and to simulate the change of stellar structures due to the shock heating. MESA cannot simulate stripping process but can be used to calculate the evolution of a star with high mass-loss rate. Following Podsiadlowski (2003), we assume that the impact of CCSNe on the companion star can be divided into two phases. In the first phase, the companion star loses mass at a very high rate ($\sim 10^{-2} - 10^{-3} M_\odot \text{yr}^{-1}$) until the mass lost equals M_{st} given by Eq. (4). This means that its thermodynamic equilibrium is destroyed at such high mass-loss rate. The result is that both the stellar radius and the rotational velocity at the stellar surface decrease as the stellar mass decreases. In the second phase, the mass loss stops but the companion star is irradiated by external heating source until $E_{\text{tot}} = 0$ at the stellar surface. In fact, similar work was done by Shappee et al. (2013) using MESA code but without considering the stellar rotation. Here, we must note that it is still different even when an additional heating source is introduced to simulate the shock heating due to the interaction between SN ejecta and a companion star. As shown by Pan et al. (2012), Liu et al. (2013) and Hirai et al. (2014), the internal structures of a star are strongly affected while the shock is passing through the star. However, in our model, the internal structures of massive stars are not affected by such interaction.

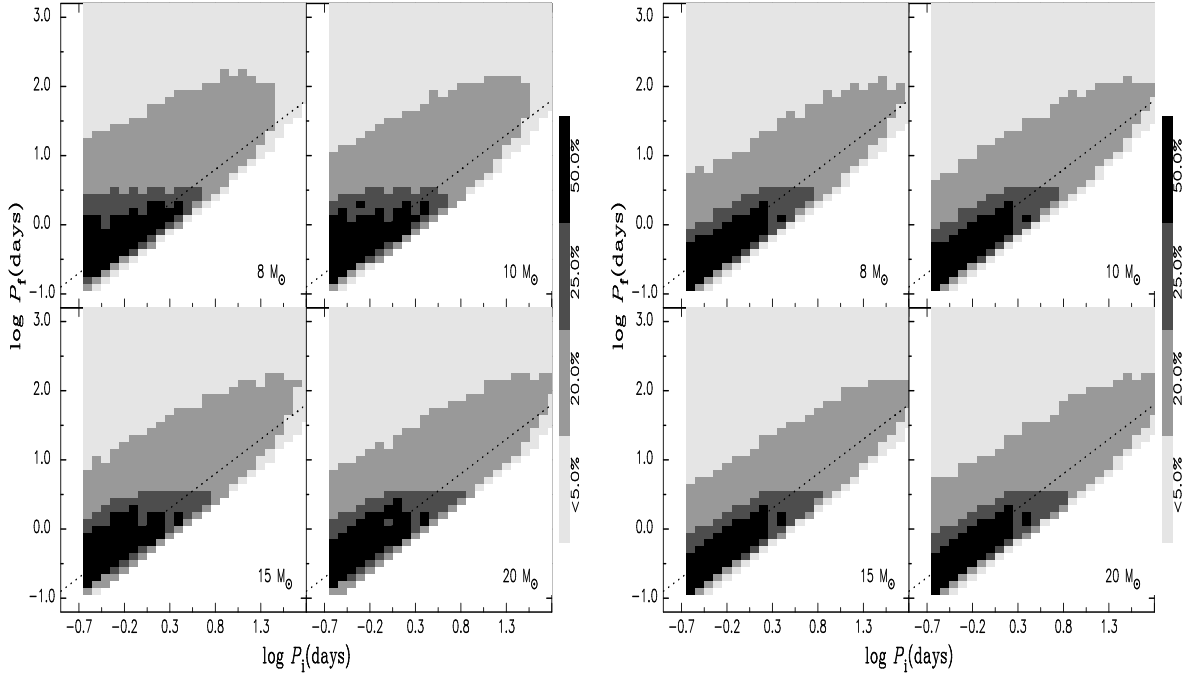


Figure 4. The distribution of pre- and post-CCSN orbital periods. The COs are NSs and BHs in the left and right panels, respectively. P_i is the pre-CCSN orbital period, while P_f is the post-CCSN orbital period. The dotted line indicates $P_i = P_f$.

Figure 5 shows an example for the evolutions of a MS companion star with mass of $10 M_\odot$ in the different phases mentioned above. When the central hydrogen abundance of the MS decreases to 90% of its initial value (its age is about 4.2547×10^6 year), the impact of CCSN begins. Based on our assumptions, the MS loses mass at a rate of $\sim 10^{-3} M_\odot \text{ yr}^{-1}$ at first. If the mass-loss rate is higher, MESA code stops due to the convergence problem. During this phase, the effective temperature, the stellar radius, the stellar luminosity and the rotational velocity drop along with the mass lost. When the stellar mass reduces to $9 M_\odot$, the mass-loss phase stops and the MS enters the irradiated phase. In this example, a value of $10^{20} \text{ erg s}^{-1} \text{ cm}^{-2}$ is assumed for the energy flux that irradiates the MS from the heating source, which means that the power of total irradiation energy is about $4.3 \times 10^{43} \text{ erg s}^{-1}$ at the beginning of the irradiated phase. As Figure 5 shows, the stellar radius increases rapidly as a result of the irradiation, which leads to great enhancement on the power. With the increase of the radius and the temperature, E_{in} becomes higher and higher but $|E_{\text{gr}}|$ becomes smaller and smaller around the stellar surface. After about 8000 seconds (equivalent to energy of about 10^{46} erg deposited into the stellar envelope), the $E_{\text{tot}} \geq 0$ at the stellar surface and the irradiated phase stops.

According to Hirai et al. (2014) and Liu et al. (2015), the stripped mass from the companion star of CCSN progenitor is determined by its mass, radius, rotating

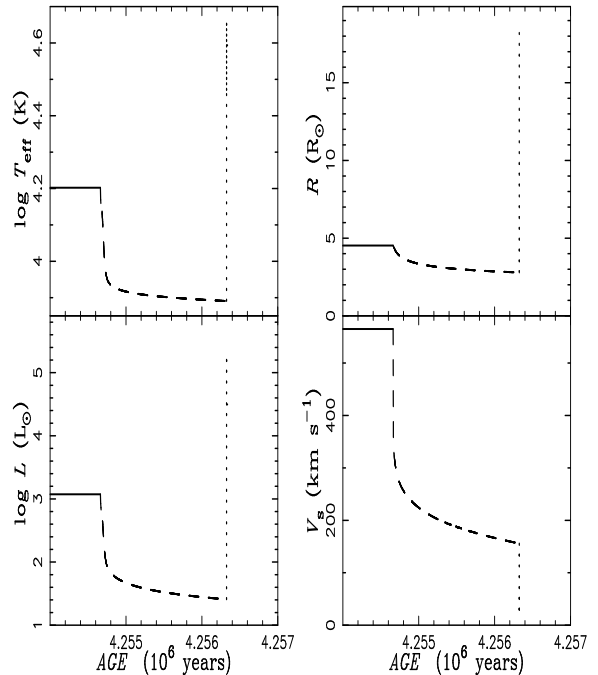


Figure 5. The evolution of the MS companion star with mass of $10 M_\odot$ during different phases. The solid, dashed and dotted lines represent the normal phase, mass-loss phase with a very high rate and irradiated phase, respectively. See text for more details.

velocity and binary separation. As shown in Figure 2, both the radius and rotating velocity change with stellar evolution. Therefore, the stripped masses depend indirectly on the stellar age. We use the mass fraction

of central hydrogen (XH) to represent the stellar age, where $XH = 0.9XH_i$ and $XH = 0.1XH_i$ represents young and old stars, respectively. Using MESA, we simulate evolution for stars with initial masses of 8, 10, 15 and $20M_\odot$, respectively. Their initial rotational velocities on the stellar surface are $0.95 V_{\text{crit}}$, $0.85 V_{\text{crit}}$ and 0. We select two points in time, at $XH = 0.9XH_i$ and $XH = 0.1XH_i$, on MS phase for discussion of the effects of stellar evolutions. Table 1 gives the radii of the MS stars for different masses and rotation velocities at the two time points.

Assuming that the mass of NS progenitor in CCSN is $8M_\odot$ allows us to estimate the stripped masses from these stars in binary systems with different pre-CCSN orbital periods. Based on Figure 6, compared to the model for non-rotating stars, the stripped mass in the model for rapid rotation stars ($V_s = 0.95V_{\text{crit}}$) is enhanced within a factor of about 2.3. As shown in Table 1, the stellar radii of the former is about 1.3 times larger than that of the latter, which results in the increase of 1.6 and 2.3 for the fitting parameters in Liu et al. (2015) and Hirai et al. (2014), respectively (See Eq. (3)). Compared to young massive stars ($XH = 0.9XH_i$) with high rotational velocity, CCSN ejecta can strip more matter from the evolved massive stars ($XH = 0.1XH_i$) because the stellar radius increases by a factor of about 2 from the time point of $XH = 0.9XH_i$ to that of $XH = 0.1XH_i$. According to our calculations, the stripped masses in the model with $XH = 0.1XH_i$ are about 6–20 times larger than that with $XH = 0.9XH_i$.

The stripped mass greatly depends on the orbital period. Figure 4 shows that HMXBs with orbital periods shorter than 10 days originate from pre-CCSN binaries with orbital periods shorter than 30 days. Based on the Figure 6, we find that, regardless of whether using fitting parameters in Hirai et al. (2014) or using those in Liu et al. (2015), the stripped masses from rotating massive stars in pre-CCSN binaries with orbital period shorter than 30 days are larger than $\sim 10^{-3}M_\odot$, and even up to several M_\odot .

4. EVOLUTION OF ROTATING MASSIVE STARS AFTER THE IMPACT

According to Hirai et al. (2014) and Liu et al. (2015), the timescale, t_{st} , for mass stripping during CCSN, is several hours. The distribution of angular momentum within the star may depend on the Eddington-Sweet circulation (Zahn 1992), whose timescale is given by

$$t_{\text{ES}} \sim t_{\text{KH}} \left(\frac{\Omega_{\text{crit}}}{\Omega} \right)^2, \quad (5)$$

where t_{KH} is the local thermal timescale. It is apparent that $t_{\text{ES}} \sim t_{\text{KH}}$ for Be stars ($\Omega \sim \Omega_{\text{crit}}$). For massive stars on MS phase, $t_{\text{KH}} \sim 10^4 - 10^5$ years (Heger et al.

2000), which means that t_{ES} is much longer than t_{st} . Therefore, the internal profiles of rotational velocity and angular momentum for rotating stars do not change when their matter is stripped during CCSNe. After a certain amount of mass is stripped from a star, its thermodynamic equilibrium is disrupted. A new equilibrium will be reached after an adjustment within a thermal timescale, during which the angular momentum within the star redistributes. After the rotating star reaches a new thermodynamic equilibrium, it begins to evolve as a non-Be star.

4.1. Evolution of Rotational Velocity

Figure 7 shows the internal profiles of rotational velocity and angular momentum (J_{spin}) from stellar surface to center. It is obvious from the figure that the rotational velocity decreases rapidly when the stellar-mass coordinates from the surface to the sub-surface. This means that the rotational velocity on the stellar surface also decreases as the stellar matter being stripped. From the left panels in Figure 7, a rapidly rotating star ($V_s = 0.95V_{\text{crit}} \sim 600\text{km s}^{-1}$) turns into a non-Be star with low rotational velocity ($V_s \sim 300\text{km s}^{-1}$) even though only a mass of $10^{-3}M_\odot$ is stripped away. However, stellar rotational velocity depends on the stellar angular momentum. Compared the right panel with the left panel in Figure 7, the degree of reduce in angular momentum is much lower than that in the rotational velocity if a certain mass is stripped away from a star. A problem appears: Is a Be star still a Be star after a certain amount of mass is stripped?

In order to answer this problem, we investigate the rotational velocity evolution of rotating star after a certain mass is stripped. In this work, we roughly divide the rotational velocity evolution of rotating star stripped mass into three phases:

- (i) Impact phase. This phase includes the stripped and the irradiated phases described in §3.2
- (ii) Thermally adjusting phase. After the impact, the heating source disappears, and the star undergoes adjustment to reach a new thermodynamic equilibrium. This phase lasts for a thermal timescale. According to Heger et al. (2000), the secular shear instability, Eddington-Sweet circulation and the Goldreich-Schubert-Fricke instability begin to drive the distribution of angular momentum on a thermal timescale, and they are secular processes. Therefore, during this phase, the above three instabilities do not work, but dynamical shear instability and Solberg-Hiløland instability affect the distribution of angular momentum.
- (iii) Normal phase. The rotating star begins to evolve into a non-Be star after it reaches a new thermodynamic equilibrium.

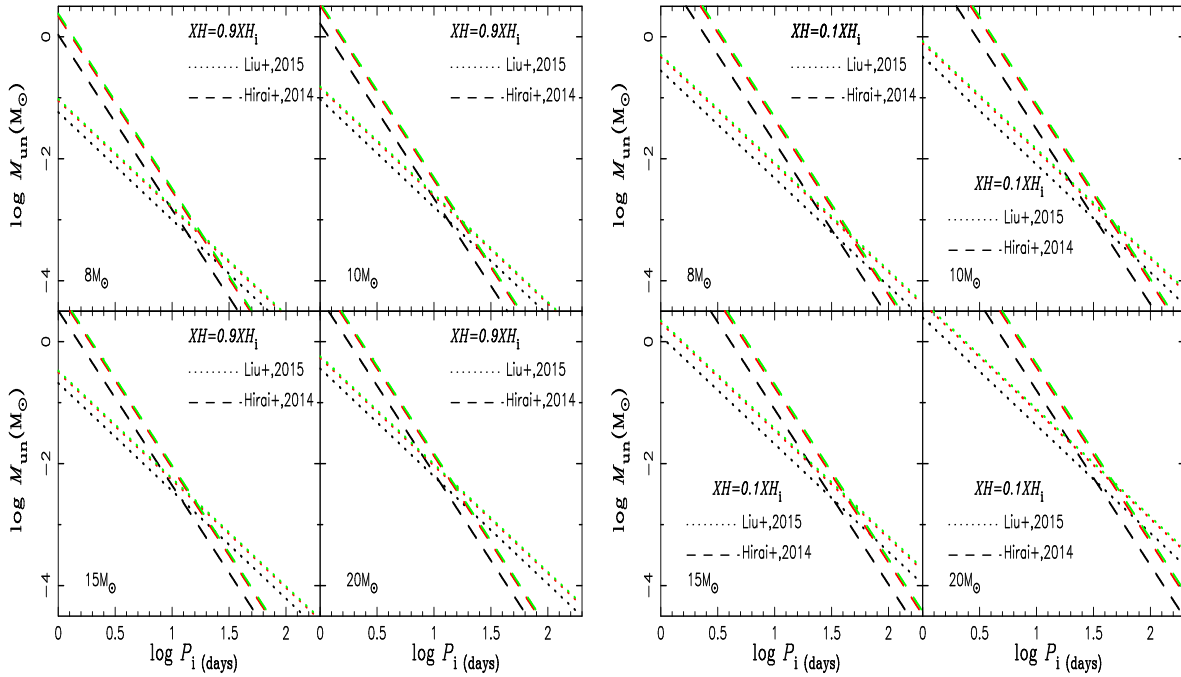


Figure 6. Stripped masses (M_{un}) vs. pre-CCSN orbital periods. The dashed and dotted lines represent the fitting parameters A and η taken from Hirai et al. (2014) and Liu et al. (2015), respectively. Lines of the same type but in different colors signify $V_i = 0$ (Black), $0.85V_{\text{crit}}$ (red) and $0.95V_{\text{crit}}$ (green), respectively. The left and right panels represent different occurring time for CCSNe when the mass fractions of central hydrogen of companion stars are 0.9 and $0.1XH_i$, respectively, where XH_i is the initial mass fractions of central hydrogen.

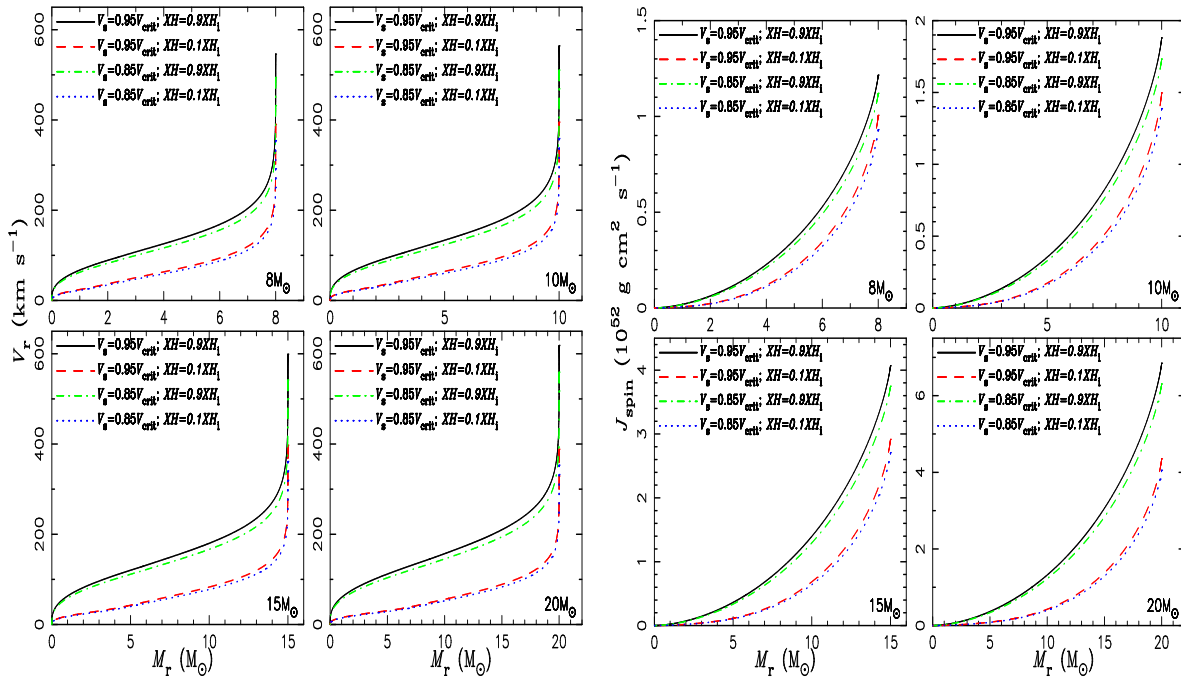


Figure 7. The internal profiles for rotational velocity (left panel) and angular momentum (right panel) vs. mass, that coordinates from stellar surface to center, of different stellar mass types with different rotational velocities and evolutionary ages.

Table 1. The radii of the MS stars for different masses and rotation velocities at $XH = 0.9XH_i$ and $XH = 0.1XH_i$, respectively. The first column gives the stellar mass when CCSNe occur. The stellar ages are given in columns 2 and 6. The stellar radii are shown from columns 3 to 5 and 7 to 9. The numbers in square brackets from columns 3 to 5 and 7 to 9 are the rotational velocity.

M (M_\odot)	$XH = 0.9XH_i$				$XH = 0.1XH_i$			
	AGE (10^6 yr)	$R(R_\odot)$ [V_s (km s $^{-1}$)]			AGE (10^7 yr)	$R(R_\odot)$ [V_s (km s $^{-1}$)]		
		$V_s = 0$	$V_s = 0.85V_{\text{crit}}$	$V_s = 0.95V_{\text{crit}}$		$V_s = 0$	$V_s = 0.85V_{\text{crit}}$	$V_s = 0.95V_{\text{crit}}$
8	6.0	3.44 [0]	4.06 [491]	4.15 [543]	2.9	6.22 [0]	7.56 [351]	9.79 [387]
10	4.3	3.95 [0]	4.63 [507]	4.74 [560]	2.0	7.24 [0]	8.78 [355]	9.04 [390]
15	2.1	4.97 [0]	5.80 [538]	5.93 [594]	1.1	9.69 [0]	11.73 [358]	12.09 [391]
20	1.5	5.86 [0]	6.81 [554]	6.97 [613]	0.8	12.11 [0]	14.83 [346]	15.30 [380]

Figure 8 gives the evolution of V_s and J_{spin} for the above three phases for a star of $10M_\odot$ with stripped mass of $1M_\odot$. At the beginning, the star is on MS phase with the abundance of hydrogen at the center (XH) is 0.9 times of the initial hydrogen abundance (XH_i), and $V_s = 0.95V_{\text{crit}}$. That is, the star is a Be star. As given in Table 1, the age, radius and rotational velocity of the star are, respectively, about 4.3×10^6 yr, $4.74 R_\odot$ and 560 km s^{-1} at this time, and, based on Figure 6, it may exist in a binary system with the orbital period shorter than 1 day.

At the beginning of the impact phase, the Be star has a high mass-loss rate (about $10^{-2} - 10^{-3} M_\odot \text{ yr}^{-1}$) so that the stellar angular momentum cannot be redistributed in a short timescale of about $10^2 - 10^3$ yr. Therefore, V_s and J_{spin} decrease rapidly as the stripped matter increases. Meanwhile, the stellar radius also reduces quickly enhancing the critical rotational velocity. Soon, the star is no longer a Be star but turns into a non-Be star. At the end of the stripped phase, the V_s and J_{spin} decrease from about 560 to 200 km s^{-1} and from about 1.87×10^{52} to $1.29 \times 10^{52} \text{ g cm}^2 \text{ s}^{-1}$, respectively. Our simulation shows that the high mass-loss phase only lasts for hundreds or thousands of years. After that, the star, having been stripped with a mass of $1 M_\odot$, is irradiated by a heating source. Its envelope rapidly expands, and its radius sharply increases while the rotational velocity on the surface drops radically. However, as Figure 9 shows, the irradiation only affects the structure near the stellar surface.

Entering the thermally adjusting phase, the mass-loss rate reduces down to normal value (about $10^{-8} M_\odot \text{ yr}^{-1}$) and the irradiation stops. The star begins to contract reaching a new thermodynamic equilibrium. From Figure 9, its radius reduces from about $20R_\odot$ to $10 R_\odot$. Due to the low mass-loss rate and the relative short timescale, J_{spin} remains almost a constant implying that the angular velocity decreases by 2.3 times. However, the star remains in the solid-body rotation because of the existence of Spruit-Tayler magnetic fields, which results in the increase of V_s . This phase lasts for about 10^4 years.

After the rapidly expanding phase, the star begins to evolve into a non-Be star. The J_{spin} and V_s decrease because of the matter lost taking away the angular momentum. However, as the star expands, V_{crit} decreases more quickly than V_s . Then, at about 1.2×10^7 years, when $V_s > 0.8V_{\text{crit}}$, the star becomes a Be star.

We calculate the evolution of V_s for stars with stripped masses of $10^{-3}M_\odot$, $10^{-2}M_\odot$, $1M_\odot$ and 25% of stellar mass at different evolutionary ages. Compare to the old Be stars given in the right panel of Figure 10, the young Be stars in the left panel of Figure 10 are more difficult

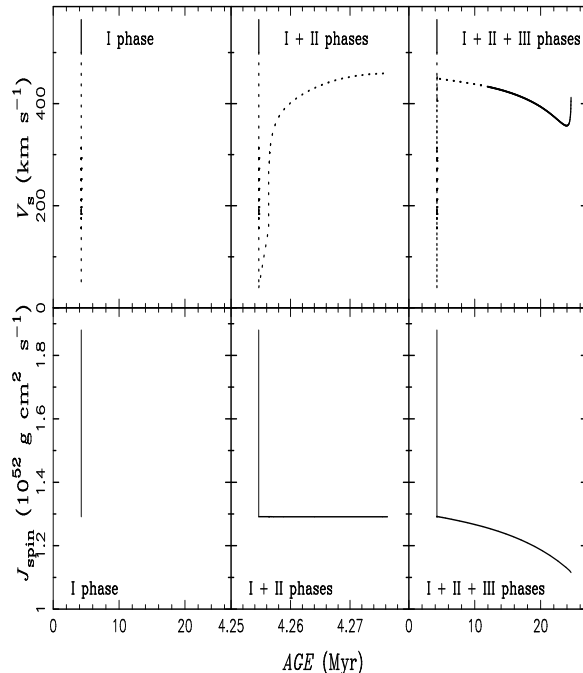


Figure 8. The evolution of rotational velocity on the stellar surface and angular momentum of star during impact, thermally adjusting and normal phases for a star of $10M_\odot$ with stripped mass of $1M_\odot$. The left panel is for phase I (the impact phase), the middle panel is for phases I and II (the impact and the thermally adjusting phases), and the right panel is for phases I, II and III (the impact, the thermally adjusting and the normal phases). The solid lines on the top three panels represent Be star ($V_s > 0.8V_{\text{crit}}$), while the dotted lines represent non-Be star ($V_s < 0.8V_{\text{crit}}$).

to turn into non-Be stars for the same stripped mass. The main reason is shown in the right panel of Figure 7: the ratio of the angular momentum taken away by the matter stripped near the stellar surface to the total angular momentum of the old Be stars is higher than that for the young Be stars. The same reason can also be used to explain why Be stars with higher mass are more difficult to evolve into non-Be stars than their lower mass counterpart. In short, a Be star with a certain amount of mass stripped can hardly evolve into a non-Be star unless the stripped mass is larger than $1 M_\odot$, even 25% of its mass.

4.2. Discussions

As shown in Figure 6, a significant amount of mass (\sim several M_\odot) should have been stripped from the progenitors of CO companions during CCSNe for HMXBs with very short orbital periods (~ 1 days). Therefore, these companions may be hydrogen-depleted objects. In known HMXBs, the orbital period of Cygnus X-3 is the shortest ($P_{\text{orb}} = 0.2$ day). Although the nature of its CO (NS or BH) is still in debate, its optical counterpart, V1521 Cyg, is a Wolf-Rayet star of the WN type (van Kerkwijk et al. 1992; Fermi LAT Collaboration et al. 2009). It means

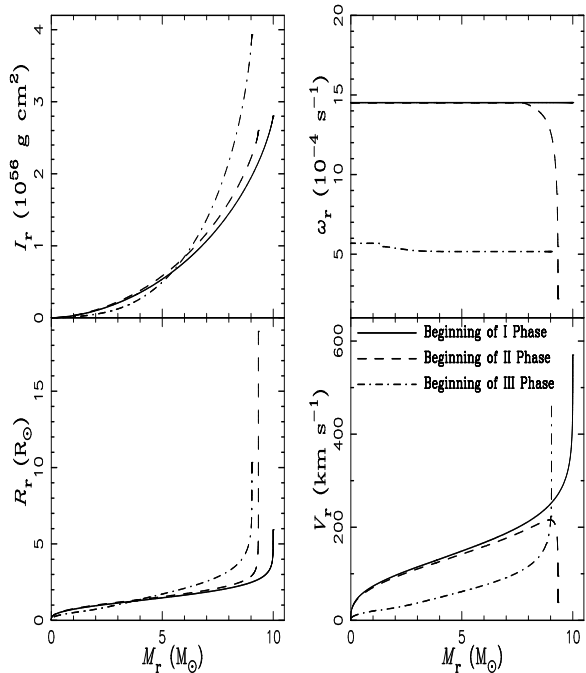


Figure 9. The internal profiles for physical parameters vs. mass coordinate (M_r) from stellar surface to center at the beginning of the three phases for a star of $10M_\odot$ mass and stripped mass of $1M_\odot$. The parameters I_r , ω_r , R_r and V_r are the moment of inertia, angular velocity, radius and rotational velocity at M_r , respectively. The phases I, II and III indicate the impact, the thermally adjusting and the normal phases, respectively.

that V1521 Cyg is helium-rich star. Based on the ionisation structure of the wind from Cygnus X-3, Terasawa & Nakamura (1994) estimated that the mass for V1521 Cyg was about $7^{+3}_{-2}M_\odot$. Compare to the typical mass of Wolf-Rayet stars, the progenitor of V1521 Cyg must have lost enormous mass via stellar wind or Roche lobe overflow (RLOF)(e. g., Lommen et al. 2005). However, in our work, its progenitor may have undergone different evolutions. As shown Figure 4 in for the changes of pre- and post-CCSN orbital periods, the progenitor system should have an orbital period shorter than ~ 1 day in order to form a HMXB with a short orbital period similar to that of the Cygnus X-3 after the CCSN explosion. We can estimate, based on Figure 6, that the stripped mass from the progenitor of V1521 Cyg could reach about $10 M_\odot$ during CCSN process. Therefore, the mass of Cyg progenitor might be $\sim 20M_\odot$ implying that most of its hydrogen-rich envelope might be blown away when the CO of Cygnus X-3 was formed.

Similarly, IWGA J0648-4119 also has a very short orbital period ($P_{\text{orb}} = 1.55$ days) implying that its

CO is likely a NS, but the massive white dwarf cannot be excluded(Mereghetti et al. 2016). Its optical counterpart, HD 49798, is a hot subdwarf of O6 spectral type with a mass of $1.50M_\odot$ (Mereghetti et al. 2009). Hot subdwarfs are core-helium-burning stars with very thin hydrogen envelope whose mass is lower than $0.01 M_\odot$ (Heber 2009). Hot subdwarfs in binary systems originate from the common-envelope ejection or stable RLOF(Han et al. 2002). Based on Figure 4, our models predict that the pre-SN progenitor system should have an orbital period shorter than ~ 3 day in order to form a HMXB with a short orbital period similar to that of the IWGA J0648-4119 after the CCSN explosion. It is possible that several M_\odot was stripped away from the progenitor of HD 49798 when it evolved into the later phase in the MS or the Hertzsprung gap. Considering the mass of HD 49798 is only about $1.50 M_\odot$, we estimate that its progenitor should have a mass of about $10M_\odot$.

5. CONCLUSIONS

We have estimated the stripped masses from rotating stars based on the fitting formula given by Hirai et al. (2014) and Liu et al. (2015) together with the observational data for HMXB orbital periods. Our results show that the amount of mass stripped is greatly dependent on the orbital periods similar to that given in the previous literatures. However, the rotational velocity introduces an uncertainty up to a factor of about 2. We focus on the evolutions of the rotational velocities, and divide the evolutions into three phases: the impact, thermally adjusting and normal phases. We find that a Be star can evolve into a non-Be star if it is stripped with a mass higher than about $1 M_\odot$.

Based on the observed orbital periods, we estimate that a mass of several M_\odot should have been stripped from V1521 Cyg and HD 49798. They are the optical counterparts of Cygnus X-3 and IWGA J0648-4119, respectively, and both are hydrogen depleted. It is probable that the whole hydrogen-rich envelopes of their progenitors might have been stripped when the COs form.

ACKNOWLEDGMENTS

GL thanks Dr Rai Yuen for polishing the English language of the manuscript. This work was supported by XinJiang Science Fund for Distinguished Young Scholars under No. 2014721015, the National Natural Science Foundation of China under Nos. 11473024, 11363005 and 11163005.

REFERENCES

Antoniou, V., & Zezas, A. 2016, ArXiv e-prints, arXiv:1603.08011

Asplund, M., Grevesse, N., & Sauval, A. J. 2005, in Astronomical Society of the Pacific Conference Series, Vol. 336, Cosmic Abundances as Records of Stellar Evolution and Nucleosynthesis, ed. T. G. Barnes, III & F. N. Bash, 25

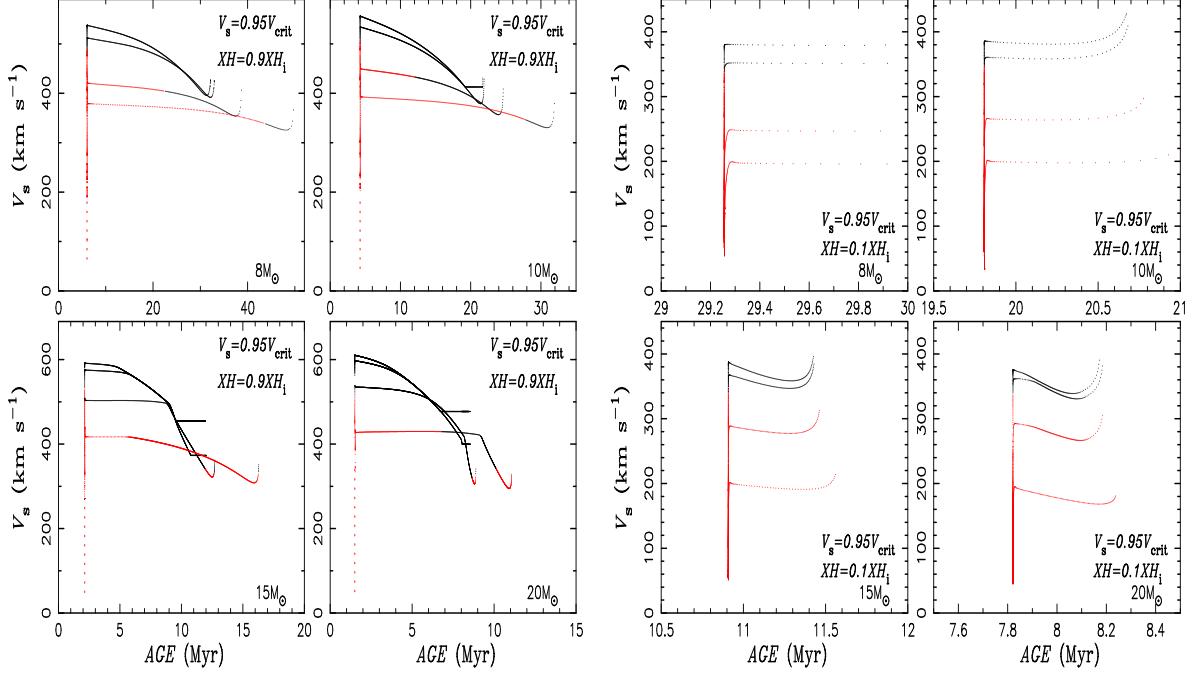


Figure 10. The evolutions of rotational velocity on the stellar surface for stars with initial masses of 8, 10, 15 and 20 M_{\odot} . The left and right panels are for different evolutionary ages at $XH = 0.9XH_i$ and $XH = 0.1XH_i$, respectively. The four dotted lines represent, from the top to the bottom, $10^{-3}M_{\odot}$, $10^{-2}M_{\odot}$, $1M_{\odot}$ and 25% of stellar mass stripped, respectively. The black and red dots mean that the stars are Be stars ($V_s > 0.8V_{\text{crit}}$) and non-Be stars ($V_s < 0.8V_{\text{crit}}$), respectively. Every dot represents a model calculated by MESA.

- Belczynski, K., Kalogera, V., Rasio, F. A., et al. 2008, *ApJS*, 174, 223
- Brandt, N., & Podsiadlowski, P. 1995, *MNRAS*, 274, 461
- Brott, I., de Mink, S. E., Cantiello, M., et al. 2011, *A&A*, 530, A115
- Chaty, S. 2013, *Advances in Space Research*, 52, 2132
- Crowther, P. A. 2007, *ARA&A*, 45, 177
- de Mink, S. E., Langer, N., Izzard, R. G., Sana, H., & de Koter, A. 2013, *ApJ*, 764, 166
- Endal, A. S., & Sofia, S. 1978, *ApJ*, 220, 279
- Fermi LAT Collaboration, Abdo, A. A., Ackermann, M., et al. 2009, *Science*, 326, 1512
- Haberl, F., & Sturm, R. 2016, *A&A*, 586, A81
- Han, Z., Podsiadlowski, P., Maxted, P. F. L., Marsh, T. R., & Ivanova, N. 2002, *MNRAS*, 336, 449
- Heber, U. 2009, *ARA&A*, 47, 211
- Heger, A., Langer, N., & Woosley, S. E. 2000, *ApJ*, 528, 368
- Hirai, R., Sawai, H., & Yamada, S. 2014, *ApJ*, 792, 66
- Hobbs, G., Lorimer, D. R., Lyne, A. G., & Kramer, M. 2005, *MNRAS*, 360, 974
- Hurley, J. R., Tout, C. A., & Pols, O. R. 2002, *MNRAS*, 329, 897
- Kudritzki, R. P., & Reimers, D. 1978, *A&A*, 70, 227
- Langer, N. 1998, *A&A*, 329, 551
- Lattimer, J. M., & Prakash, M. 2007, *PhR*, 442, 109
- Liu, Q. Z., van Paradijs, J., & van den Heuvel, E. P. J. 2006, *A&A*, 455, 1165
- Liu, Z.-W., Tauris, T. M., Röpke, F. K., et al. 2015, *A&A*, 584, A11
- Liu, Z.-W., Pakmor, R., Seitenzahl, I. R., et al. 2013, *ApJ*, 774, 37
- Lommen, D., Yungelson, L., van den Heuvel, E., Nelemans, G., & Portegies Zwart, S. 2005, *A&A*, 443, 231
- Maeder, A., & Meynet, G. 2000, *ARA&A*, 38, 143
- Marietta, E., Burrows, A., & Fryxell, B. 2000, *ApJS*, 128, 615
- Mereghetti, S., Pintore, F., Esposito, P., et al. 2016, *MNRAS*, 458, 3523
- Mereghetti, S., Tiengo, A., Esposito, P., et al. 2009, *Science*, 325, 1222
- Nieuwenhuijzen, H., & de Jager, C. 1990, *A&A*, 231, 134
- Pan, K.-C., Ricker, P. M., & Taam, R. E. 2012, *ApJ*, 750, 151
- Parsignault, D. R., Gursky, H., Kellogg, E. M., et al. 1972, *Nature Physical Science*, 239, 123
- Paxton, B., Bildsten, L., Dotter, A., et al. 2011, *ApJS*, 192, 3
- Paxton, B., Cantiello, M., Arras, P., et al. 2013, *ApJS*, 208, 4
- Paxton, B., Marchant, P., Schwab, J., et al. 2015, *ApJS*, 220, 15
- Pinsonneault, M. H., Kawaler, S. D., Sofia, S., & Demarque, P. 1989, *ApJ*, 338, 424
- Podsiadlowski, P. 2003, *ArXiv Astrophysics e-prints*, astro-ph/0303660
- Porter, J. M., & Rivinius, T. 2003, *PASP*, 115, 1153
- Reig, P. 2011, *Ap&SS*, 332, 1
- Romano, P., Krimm, H. A., Palmer, D. M., et al. 2014, *A&A*, 562, A2
- Shao, Y., & Li, X.-D. 2014, *ApJ*, 796, 37
- Shappee, B. J., Kochanek, C. S., & Stanek, K. Z. 2013, *ApJ*, 765, 150
- Terasawa, N., & Nakamura, H. 1994, *ApJS*, 92, 477
- Thackeray, A. D. 1970, *MNRAS*, 150, 215
- van Kerkwijk, M. H., Charles, P. A., Geballe, T. R., et al. 1992, *Nature*, 355, 703
- Vassiliadis, E., & Wood, P. R. 1993, *ApJ*, 413, 641
- Vink, J. S., de Koter, A., & Lamers, H. J. G. L. M. 2001, *A&A*, 369, 574
- Wheeler, J. C., Lecar, M., & McKee, C. F. 1975, *ApJ*, 200, 145
- Yoon, S.-C., Langer, N., & Norman, C. 2006, *A&A*, 460, 199
- Zahn, J.-P. 1992, *A&A*, 265, 115

